Volume 14
Number 1
2 January 2026
Pages 1–664

Journal of Materials Chemistry A

Materials for energy and sustainability

rsc.li/materials-a

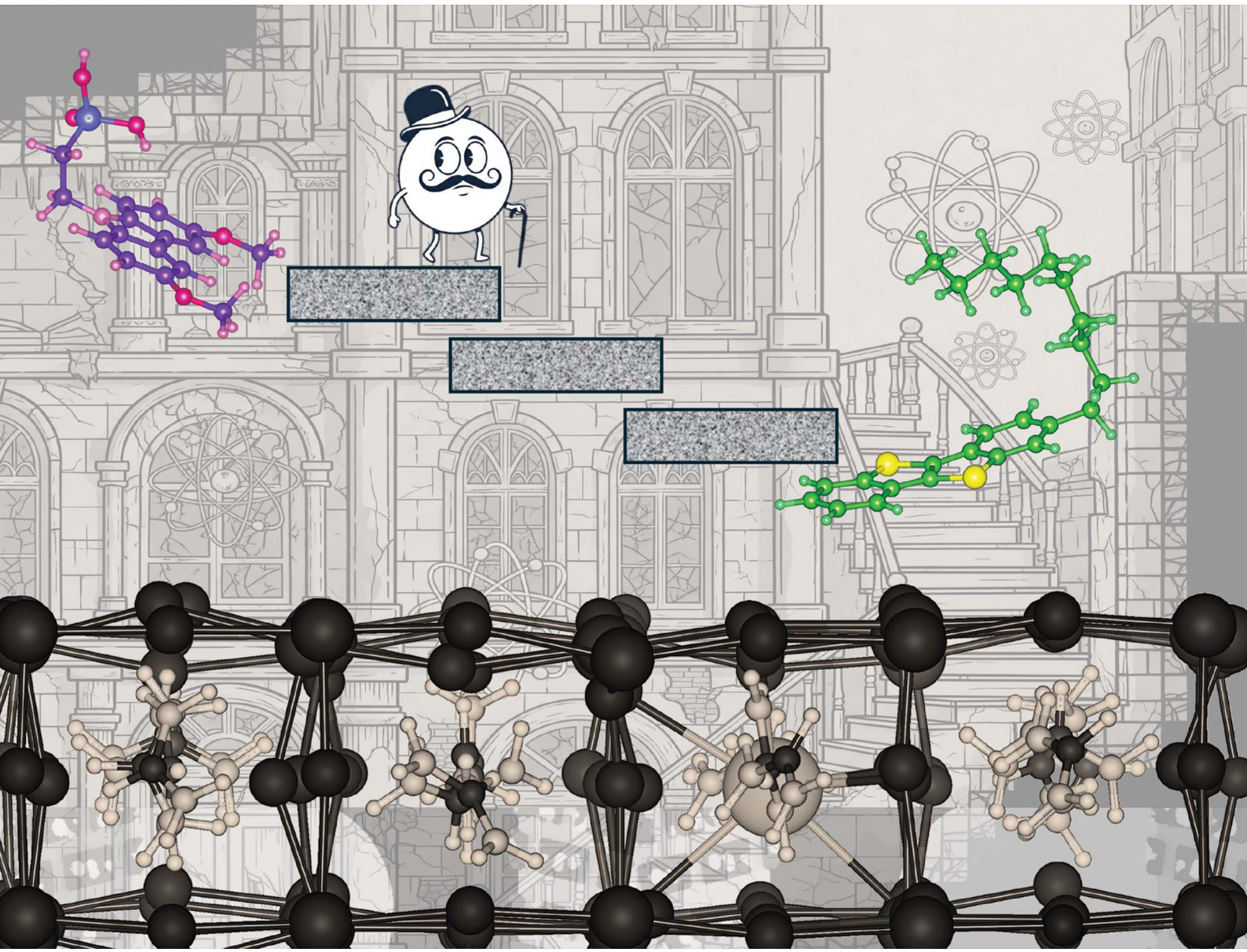

ISSN 2050-7488

ROYAL SOCIETY OF CHEMISTRY

COMMUNICATION

Ana B. Muñoz-García *et al.*

Unveiling enhanced hole transfer mechanism in perovskite solar cells with a self-assembled monolayer and [1] benzothieno[3,2-b][1]benzothiophene interlayer

Journal of Materials Chemistry A

ROYAL SOCIETY OF CHEMISTRY

COMMUNICATION

View Article Online
View Journal | View Issue

Check for updates

Cite this: *J. Mater. Chem. A*, 2026, **14**, 313

Received 13th February 2025
Accepted 17th July 2025

DOI: 10.1039/d5ta01185j

rsc.li/materials-a

Unveiling enhanced hole transfer mechanism in perovskite solar cells with a self-assembled monolayer and [1]benzothieno[3,2-b][1]benzothiophene interlayer†

Adriana Pecoraro, [a] Francesca Fasulo, [a] Michele Pavone, [b] Aldo Di Carlo [cd] and Ana B. Muñoz-García *[a]

With exceptional photoconversion efficiencies, Perovskite Solar Cells (PSCs) are shaping the future of next-generation photovoltaics. Their performance and stability critically depend on the interfaces between the photoactive perovskite and charge transport layers. Incorporating interlayer materials to fine-tune these interfacial properties has significantly improved both efficiency and durability, yet the mechanisms driving these effects remain poorly understood. In this work, we use advanced computational methods based on density functional theory to investigate the role of a C10-BTBT interlayer between a triple-cation perovskite and the widely used MeO-2PACz. Our results uncover, for the first time, a bridge-mediated charge transfer mechanism, demonstrating how C10-BTBT not only strengthens interfacial chemical interactions, but also plays a key role in accelerating hole injection. These novel insights provide a molecular-level understanding of interlayer contributions and establish a robust and versatile framework, broadly applicable to the design and optimization of PSC interfaces for enhanced efficiency and durability.

The increasing efficiencies achieved by perovskite solar cells (PSCs) represent a remarkable breakthrough in the renewable energy field. The excellent optoelectronic properties of perovskite materials enable high power conversion efficiencies comparable to traditional silicon-based solar cells, while offering the added benefits of lower manufacturing costs and the potential for flexible and lightweight designs.[1,2] Research continues to push the boundaries of PSCs efficiencies through innovative materials, fabrication techniques, and novel device architectures.[3–9] Interfacial engineering using interlayers between the active material and the charge transport layer (CTL) plays a crucial role, since interlayers control the energy level alignment, improve the contact quality between adjacent layers, reduce energy barriers for charge extraction and mitigate interfacial defects, thereby improving device performance and stability.[4,10–12] A successful strategy for perovskite/CTL interface engineering is with self-assembled monolayers (SAMs). These ultrathin, molecular layers spontaneously organize on substrates, offering precise control over surface properties. SAMs have proven particularly effective as dual-function interlayers in PSCs, offering benefits such as defect passivation, energy-level tuning, and chemical stabilization of interfaces while acting as CTLs themselves. For instance, N719 dye SAMs effectively passivate defects on both metal-oxide and perovskite surfaces while preventing harmful chemical interactions that can lead to degradation.[13] Similarly, the N749 dye has been applied at the NiO/perovskite interface in p–i–n perovskite solar cells (PSCs), where it enhances moisture stability and boosts device performance.[13] In turn, 2PACz is used to modify the work function of ITO, forming a barrier-free contact with the perovskite layer for efficient hole extraction.[13] ZnO and SnO_2 can also be optimized using SAMs or zwitterions to improve charge extraction and reduce recombination, while materials like NiO_x benefit from dipole molecules such as TPMA and 2PACz for better energy alignment and hole extraction.[4] While hole-selective SAMs are effective in some PSCs, their limited temperature stability poses severe challenges, particularly in maintaining strong adhesion between SAMs and perovskites, which can compromise the mechanical stability of PSCs under temperature fluctuations. To overcome this issue, self-assembled bilayers (SABs), composed of two distinct SAMs, have been explored. Compared to SAMs, SABs offer improved stability, greater functional versatility and precise control over film termination.[14] A functional interlayer made of 5-(trifluoromethyl)-1-benzothiophene-2-carboxylic acid (TFMBTA), has recently been introduced between MeO-2PACz hole transport layer (HTL) and the perovskite.[15] TFMBTA has

[a]Department of Physics "E. Pancini", University of Naples Federico II, 80126 Napoli, Italy. E-mail: anabelen.munozgarcia@unina.it

[b]Department of Chemical Sciences, University of Naples Federico II, 80126 Napoli, Italy

[c]CHOSE-Department of Electronic Engineering, University of Rome "Tor Vergata", 00133 Roma, Italy

[d]Istituto di Struttura Della Materia, Consiglio Nazionale Delle Ricerche, 00133 Roma, Italy

† Electronic supplementary information (ESI) available. See DOI: https://doi.org/10.1039/d5ta01185j

been found to enhance charge transfer, hole extraction, and perovskite deposition by optimizing the HTL surface morphology and energy level alignment, while its functional groups passivate perovskite defects, reducing non-radiative recombination.

Current computational literature tackles the perovskite/charge transport layers' interfaces from different perspectives. Some works mainly focus on the charge transport layers assessing their optoelectronic features along with the proper band alignment from calculations performed on isolated materials.[7,8,15–20] Other works focus on the interfaces with photoactive materials accounting for mutual polarization effects and assessing the efficiency of the charge transport at interfaces.[6,9,21–25] Some work specifically focus on SAM, investigating their role in tailoring the work function of electrodes.[26–28] Only few works investigate the effect of interlayer materials to improve the perovskite/charge transport layers interface.[11,29,30]

In a recent paper by Takhellambam *et al.*,[31] a small organic molecule (2-decyl-[1]benzothieno [3,2-b][1]benzothiophene, a.k.a. C10-BTBT) monoalkylated with a carbon linear straight chain is employed as interlayer between the MeO-2PACz SAM HTL and the triple-cation lead halide perovskite (TriLHP) $Cs_{0.05}MA_{0.15}FA_{0.80}PbI_{2.49}Br_{0.51}$ in a p–i–n architecture. The interlayer does not alter the morphology or crystal structure of the perovskite but significantly facilitates charge carrier extraction at the perovskite/HTL interface. Preliminary theoretical simulations of an isolated MeO-2PACz/C10-BTBT dyad show a co-facial arrangement that aligns their highest occupied molecular orbitals (HOMOs) and provides a slight advantage (0.1 eV) for hole collection by MeO-2PACz when paired with C10-BTBT.[31] Here, we take a significant step further by exploiting density functional theory (DFT) simulations to model the complete TriLHP/MeO-2PACz interface, with and without the C10-BTBT interlayer, and thus offering deeper insights into its role in enhancing interfacial interactions and charge transfer.

Structural model and electronic structure features of TriLHP bulk are depicted by Fig. S1 of the (ESI).† For the interfaces, we consider the thermodynamically favored (010) perovskite surface[32] with two possible terminations: the AX (with A = Cs, FA, MA) and the PbX_2 (with X = I, Br). For each termination, we consider either the MeO-2PACz SAM or the MeO-2PACz/C10-BTBT dyad.

Fig. 1 displays the minimum-energy structures of these interfaces, and the corresponding binding and adhesion energies, which are calculated as:

$$E_b = E_{int} - E_{surf} - E_{mol} \quad (1)$$

$$E_a = E_{int} - E^*_{surf} - E^*_{mol} \quad (2)$$

where the binding energy (E_b) is the difference between the total energy of the relaxed interface (E_{int}) and those of the isolated perovskite surface (E_{surf}) and molecule (E_{mol}). The adhesion energetic contribution (E_a) refers instead to the energies of the surface (E^*_{surf}) and the molecules (E^*_{mol}) at the interface minimum-energy geometry. According to these definitions, the interaction strength between the perovskite and the molecules is quantified in terms of purely electronic contribution (E_a) or encompasses also the unfavorable distortion energies of the interface components (E_b). Electronic interaction at the interface can be qualitatively analyzed by computing electron density changes upon interface formation, see Fig. 1 (lateral view) and Fig. S2 of the ESI (top view).† The interaction between both surface terminations and MeO-2PACz primarily affects the molecular π-electron systems. In the PbX_2 termination,

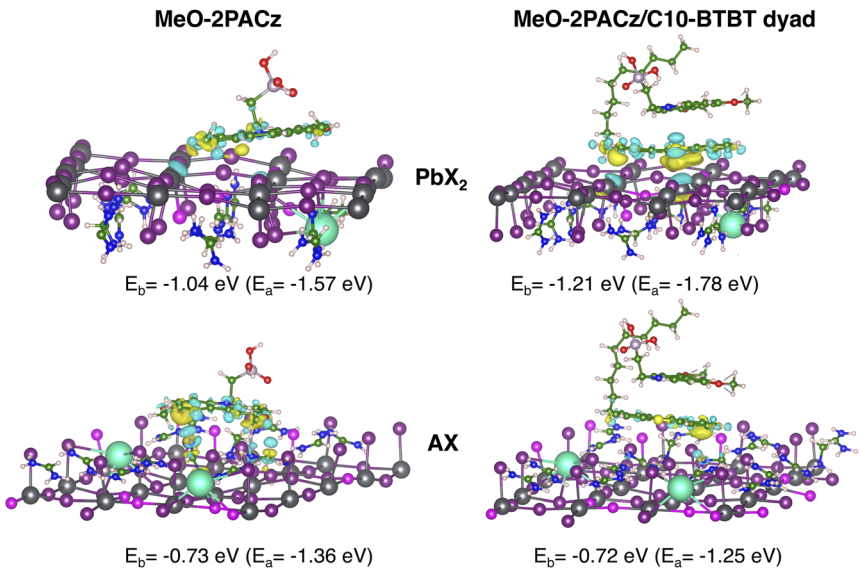

Fig. 1 Lateral views of the relaxed TriLHP/molecule(s) interfaces with AX and PbX_2 terminations. Molecule(s) refer to MeO-2PACz or to the C10-BTBT/MeO-2PACz dyad. Only the two outermost layers of the perovskite are shown for clarity. Electron density difference plots (iso-surface value = 0.005 a.u.) are shown; yellow and blue regions denote charge accumulation and depletion zones upon interface formation, respectively. Binding (E_b) and adhesion (E_a) energies calculated at the DFT-HSE06 level of theory according to eqn (1) and (2), respectively, are shown for each interface. Atomic color code: Cs, turquoise; Pb, dark gray; I, plum; Br, magenta; C, green; N, blue; H, light pink; P, lavender; O, red.

electrons accumulate on the methoxy groups, which interact with the Pb atoms of the outermost perovskite layer. In contrast, for the AX terminated slab, the π-electrons interact directly with the organic moieties (MA and FA) on the surface. A similar interaction is observed upon introduction of C10-BTBT, where the planar π-system of the interlayer molecule interacts with the Pb atoms of the PbX_2 -terminated surface and, to a much lesser extent, with the AX-terminated one. PbX_2-terminated surfaces exhibit stronger interactions with MeO-2PACz and C10-BTBT molecules compared to AX-terminated counterparts. Notably, the introduction of C10-BTBT improves the binding between PbX_2 termination and MeO-2PACz, achieving the most favorable binding energy (−1.21 eV). It is worth noticing that the interlayer does not alter the energy loss due structural distortions upon binding to the perovskite surface, being the difference between E_a and E_b constant with or without the C10-BTBT. On the other side, adding the interlayer to the AX termination has a minor impact on binding, as the chemical interactions

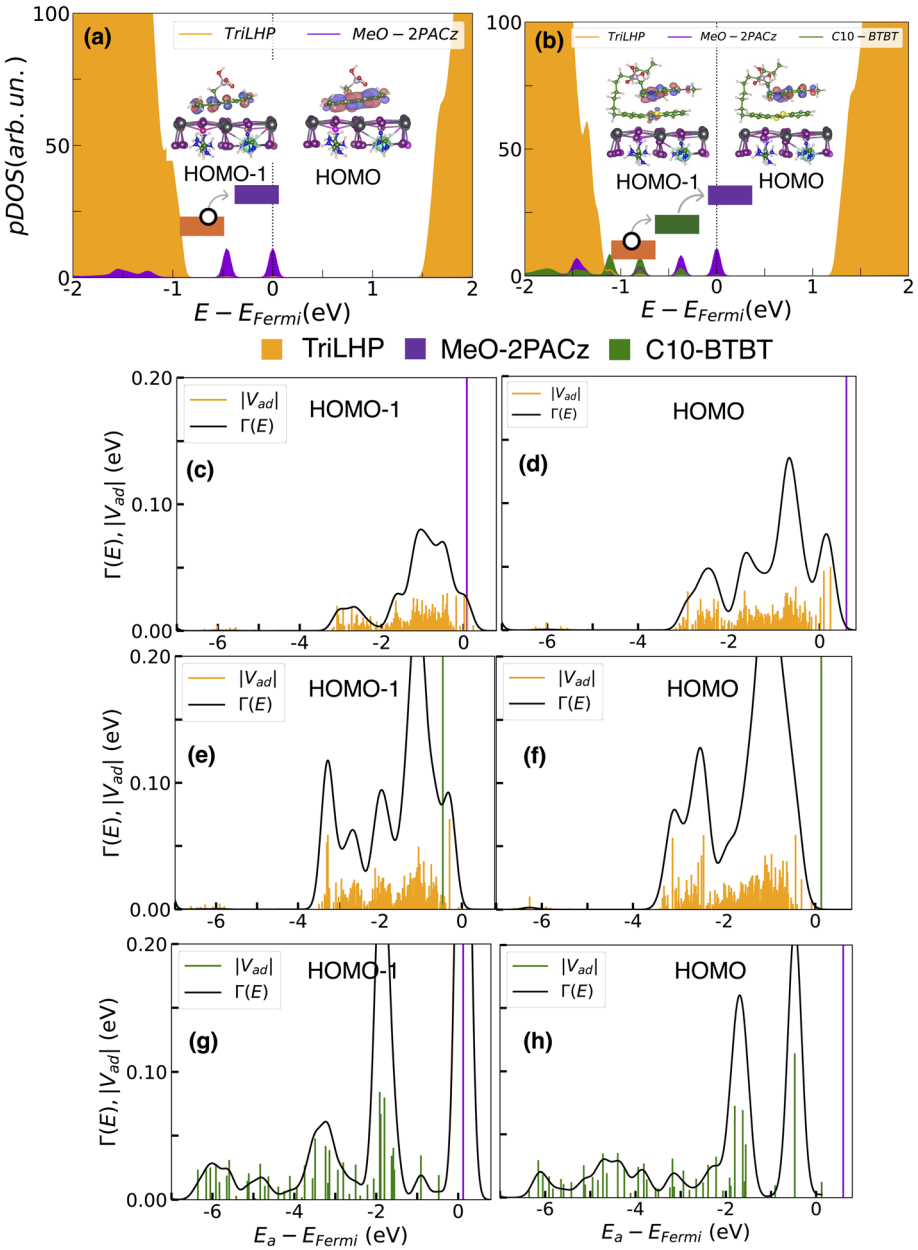

Fig. 2 DFT-HSE06 projected density of states for the PbX_2-terminted interface with MeO-2PACz (a) and dyad (b). Density of states plots are resolved for the different moieties (TriLHP, MeO-2PACz, and C10-BTBT). HOMO and HOMO-1 are depicted for each interface (isosurface value: 0.09 a.u.). Corresponding data for AX termination are in Fig. S3 of ESI.† DFT-HSE06 computed coupling matrix elements (V_{ad}), considering as donor/acceptor the couples MeO-2PACz/TriLHP (c and d), C10-BTBT/TriLHP (e and f), and MeO-2PACz/C10-BTBT (g and h) systems, for both the HOMO and HOMO-1 donor states and a wide range of acceptor states (E_a). The solid black line represents the spectral function $\Gamma(E)$ calculated according to eqn (3). In each plot, MeO-2PACz and C10-BTBT states are represented by violet and green vertical lines, respectively. The corresponding transition times for the less energetically favorable AX-terminated interface are listed in Table S1 of ESI.†

between this termination and the C10-BTBT are less favorable. In fact, the E_a for the dyad is slightly less negative that for MeO-2PACz alone. We also analyze a different model of the AX interface featuring a different population of the topmost layer. The computational models of these interfaces are shown in the ESI, Fig. S4,† together with the corresponding density of states (DOS). Adhesion energies for this model still indicate weaker interactions with the molecules. In addition, the computed DOS shows a non-ideal band alignment, suggesting limited suitability for charge transfer. Given the significant thermodynamic preference for PbX_2-terminated surfaces, and the fact that such terminations offer the most favorable conditions for efficient charge transfer and interfacial stability,[33,34] we focus our subsequent analysis of the electronic properties on the PbX_2 termination. Results for the AX-terminated surfaces are included in the ESI† for completeness. A qualitative estimate of the band alignment for the PbX_2 interface model can be derived from DOS, as shown in Fig. 2.

Computed DOS reveals a favorable band alignment between the molecule HOMO and the valence band of the perovskite. At the bare perovskite/HTL interface, both the HOMO and HOMO-1 of MeO-2PACz are positioned well above the valence band maximum (VBM) of the perovskite. Introducing the interlayer preserves this alignment and amplifies the energy difference, thereby providing a higher driving force for hole injection. In this configuration, the HOMO of the molecule remains localized on the SAM, whereas the HOMO-1 and lower energy states become delocalized across both the SAM and the interlayer. This picture is corroborated by molecular orbitals presented in Fig. 2(a and b) for the MeO-2PACz and the dyad interface, respectively.

In addition to the thermodynamic evaluation, we assess the effect of C10-BTBT on charge transport kinetics using the projection operator diabatization (POD) approach developed by Futera and co-workers.[35] This method involves projecting the Kohn–Sham Hamiltonian onto an orthogonal basis localized on both donor and acceptor atoms. In this new basis, donor–acceptor coupling elements can be isolated and the probability and characteristic time of the selected transitions can be extracted. In particular, we have computed the coupling elements at the HSE06 level of theory using the POD implementation available in CP2K.[35,36]

Fig. 2 displays the coupling elements V_{nm} between the donor (n) and the acceptor states (m) for the charge transfer processes at PbX_2/MeO-2PACz interfaces, both with and without the interlayer molecule. In the first case, we examine electron injection from the SAM to the VB states of the TriLHP. In the case with the dyad, the charge transfer process is analyzed in two steps: electron injection from MeO-2PACz to the occupied states of the interlayer, followed by injection from C10-BTBT to the perovskite. Due to the presence of several molecular states well above the VBM of the perovskite, we consider both the HOMO and HOMO-1 orbitals as potential channels for charge transfer. Characteristic times for each process are then evaluated using the spectral function ($\Gamma_n(E)$), defined as:

$$\Gamma_n(E) = 2\pi\ \Sigma_m |V_{nm}|^2\ \delta(E - \varepsilon_m) \quad (3)$$

Starting from $\Gamma_n(E)$ (eqn (3)), transitions times can be estimated through the relation $\tau = h/(2\pi \cdot \max(\Gamma))$. Calculated injection times are summarized in Table 1.

It is important to note that the calculated transition times are intended as comparative tools for evaluating charge transfer (CT) kinetics across different models, rather than as absolute values for direct comparison with experimental data. This limitation arises from the dependence of these times on the mathematical model used to approximate the delta distribution in the spectral function calculation. The fastest CT in the bare TriLHP/MeO-2PACz interface originates from the HOMO level of the molecule, with a characteristic time of 4.84 fs. In the interface incorporating C10-BTBT, an even faster CT process can occur *via* two distinct bridge-mediated pathways that occur with a first electron injection from the MeO-2PACz HOMO-1 to BTBT, followed by a second electron transfer from C10-BTBT's HOMO or HOMO-1 to the perovskite. The longer charge transfer time associated with the MeO-HOMO can be attributed to the reduced overlap of its electronic wavefunction with that of the neighboring molecule. In contrast, the HOMO-1 state—evident from the density of states (DOS) in Fig. 2b and its spatial distribution—shows localization across both molecules, indicating stronger orbital overlap. This enhanced delocalization facilitates greater electronic coupling, thereby reducing the charge transfer time. The total CT times for these pathways are 3.27 fs (1.12 fs + 2.15 fs) and 3.30 fs (1.12 fs + 2.18 fs), respectively. These two bridge-mediated mechanisms are indeed more favorable than the direct CT process computed for the TriLHP/MeO-2PACz interface. The computed faster injection, aligning with the experimental findings (time-resolved photoluminescence measurements) with the dyad by Takhellambam *et al.*,[31] supports the hypotheses that the two-step mechanism drives the interfacial CT process. For this surface termination, the fastest computed time corresponds to the electron injection from the HOMO-1 of MeO-2PACz to the perovskite. Moreover, the improved strength of the MeO-2PACz/TriLHP interface, led

Table 1 Charge transfer times for the TriLHP/MeO-2PACz and the full TriLHP/dyad interfaces with PbX_2 termination, calculated at DFT-HSE06 level from $\Gamma_n(E)$ (eqn (3))

Interface	TriLHP/MeO-2PACz	TriLHP/C10-BTBT/MeO-2PACz	
Donor/acceptor	MeO-2PACz/TriLHP	MeO-2PACz/C10-BTBT	C10-BTBT/TriLHP
HOMO-1	8.21 fs	1.12 fs	2.18 fs
HOMO	4.84 fs	3.04 fs	2.15 fs

by the presence of the C10-BTBT interlayer can be the reason for the high fill factor found experimentally.

Further analysis of thermal fluctuations and of the effects of the diverse chemical environment (SAM, additives, surface defects) will be the next step for improving our understanding of the subtle physical-chemical features of such complex functional interface. We will pursue these investigations with theoretical modeling approaches exploiting molecular dynamics, which can be very effective for revealing the relationships between chemical composition, defect states, and charge transport properties.[37]

In conclusion, our theoretical modeling of the TriLHP/C10-BTBT/MeO-2PACz interface provides new atomistic insights into the role of C10-BTBT in enhancing charge transfer. Our DFT results highlight the influence of the specific termination of the (010)-surface of the perovskite on the interface stability, as reflected in both binding and adhesion energies. In particular, the PbX_2 termination is the most favorable for MeO-2PACz binding, with C10-BTBT further stabilizing the perovskite/HTL interface. This stabilization arises from the interaction of the delocalized π-electrons of C10-BTBT with surface lead atoms.

Beyond stability, the C10-BTBT interlayer significantly impacts electronic properties by inducing a shift in the molecule's frontier orbitals relative to the perovskite valence band, thereby increasing the driving force for hole transfer. Moreover, the interlayer enhances charge transfer kinetics, as evidenced by faster injection times. A comparison of charge transfer times at the bare MeO-2PACz/perovskite interface and the two-step mechanism mediated by C10-BTBT reveals that this bridge-mediated transfer mechanism is the most plausible explanation for the observed improvement in hole transfer rates.

Overall, the proposed computational protocol offers an effective and practical theoretical framework to evaluate SABs and investigate the role of interlayers in strengthening SAM binding to perovskite layers and improving charge extraction. It provides a feasible and systematic approach to assess various bilayer configurations, offering a valuable tool for the rational design of optimized interfaces to enhance the performance and stability of PSCs.

Methods and computational details

All-electron DFT[38] calculations with periodic boundary conditions (PBC) are performed using basis set of numerical atom-centered orbitals (NAO),[39] as implemented in the Fritz Haber Institute *ab initio* molecular simulations (FHI-aims) code.[40] Within the FHI-aims framework, electrons have been described by the zero-order regular approximation (atomic ZORA). A threshold of 1×10^{-6} eV has been employed for self-consistency convergence of the total energy. The Perdew–Burke–Ernzerhof, PBE[41] exchange correlation functional has been employed for all geometry optimizations including the Tkatchenko–Scheffler (TS) correction[42] accounting for van der Waals dispersion forces. Structures have been fully relaxed until maximum forces acting on each atom were below 0.02 eV $Å^{-1}$. All calculations have been performed in the Γ point of the Brillouin zone. The light-tier1 basis of NAO was used for structural relaxations. Electronic calculations have been refined by means of the HSE06 (REF) hybrid functional to calculate the projected density of states (pDOS). This electronic analysis together with calculation of electronic couplings has been performed through the CP2k software.[35]

Data availability

The data supporting this article have been included as part of the ESI.†

Conflicts of interest

There are no conflicts to declare.

Acknowledgements

This study was carried out within the NEST – Network for Energy Sustainable Transition and received funding from the European Union Next-Generation EU (PIANO NAZIONALE DI RIPRESA E RESILIENZA (PNRR) – MISSIONE 4 COMPONENTE 2, INVESTIMENTO 1.3). This manuscript reflects only the authors' views and opinions; neither the European Union nor the European Commission can be considered responsible for them. We also acknowledge the support of MASE (Ministero dell'Ambiente e della Sicurezza Energetica) in the framework of the Operating Agreement with ENEA for Research on the Electric System.

References

1 R. Sharif, A. Khalid, S. W. Ahmad, A. Rehman, H. G. Qutab, H. H. Akhtar, K. Mahmood, S. Afzal and F. Saleem, A Comprehensive Review of the Current Progresses and Material Advances in Perovskite Solar Cells, *Nanoscale Adv.*, 2023, **5**(15), 3803–3833, DOI: **10.1039/D3NA00319A**.

2 G. Szabó, N.-G. Park, F. De Angelis and P. V. Kamat, Are Perovskite Solar Cells Reaching the Efficiency and Voltage Limits?, *ACS Energy Lett.*, 2023, **8**(9), 3829–3831, DOI: **10.1021/acsenergylett.3c01649**.

3 A. Abate, Stable Tin-Based Perovskite Solar Cells, *ACS Energy Lett.*, 2023, **8**(4), 1896–1899, DOI: **10.1021/acsenergylett.3c00282**.

4 M. Ye, C. He, J. Iocozzia, X. Liu, X. Cui, X. Meng, M. Rager, X. Hong, X. Liu and Z. Lin, Recent Advances in Interfacial Engineering of Perovskite Solar Cells, *J. Phys. D: Appl. Phys.*, 2017, **50**(37), 373002, DOI: **10.1088/1361-6463/aa7cb0**.

5 A. Bist, B. Pant, G. P. Ojha, J. Acharya, M. Park and P. S. Saud, Novel Materials in Perovskite Solar Cells: Efficiency, Stability, and Future Perspectives, *Nanomaterials*, 2023, **13**(11), 1724, DOI: **10.3390/nano13111724**.

6 C. Coppola, A. Pecoraro, A. B. Muñoz-García, R. Infantino, A. Dessì, G. Reginato, R. Basosi, A. Sinicropi and M. Pavone, Electronic Structure and Interfacial Features of Triphenylamine- and Phenothiazine-Based Hole Transport Materials for Methylammonium Lead Iodide Perovskite Solar Cells, *Phys. Chem. Chem. Phys.*, 2022, **24**(24), 14993–15002, DOI: **10.1039/D2CP01270G**.

7 G. V. Sannino, A. De Maria, V. La Ferrara, G. Rametta, L. V. Mercaldo, M. L. Addonizio, L. Lancellotti, A. Pecoraro, A. B. Muñoz-García, M. Pavone and P. Delli Veneri, Development of SnO_2 Composites as Electron Transport Layer in Unencapsulated $CH_3NH_3PbI_3$ Solar Cells, *Solids*, 2021, **2**(4), 407–419, DOI: **10.3390/solids2040026**.

8 G. V. Sannino, A. Pecoraro, P. Maddalena, A. Bruno, P. D. Veneri, M. Pavone and A. B. Muñoz-García, The Role of Mg Dopant Concentration in Tuning the Performance of the SnO_2 Electron Transport Layer in Perovskite Solar Cells, *Sustainable Energy Fuels*, 2023, **7**(19), 4855–4863, DOI: **10.1039/D3SE00362K**.

9 A. Pecoraro, A. D. Maria, P. D. Veneri, M. Pavone and A. B. Muñoz-García, Interfacial Electronic Features in Methyl-Ammonium Lead Iodide and p-Type Oxide Heterostructures: New Insights for Inverted Perovskite Solar Cells, *Phys. Chem. Chem. Phys.*, 2020, **22**(48), 28401–28413, DOI: **10.1039/D0CP05328G**.

10 J. Dagar, M. Fenske, A. Al-Ashouri, C. Schultz, B. Li, H. Köbler, R. Munir, G. Parmasivam, J. Li, I. Levine, A. Merdasa, L. Kegelmann, H. Näsström, J. A. Marquez, T. Unold, D. M. Többens, R. Schlatmann, B. Stegemann, A. Abate, S. Albrecht and E. Unger, Compositional and Interfacial Engineering Yield High-Performance and Stable p–i–n Perovskite Solar Cells and Mini-Modules, *ACS Appl. Mater. Interfaces*, 2021, **13**(11), 13022–13033, DOI: **10.1021/acsami.0c17893**.

11 A. Pecoraro, A. B. Muñoz-García, G. Sannino, P. Delli Veneri and M. Pavone, Exotic Hexagonal NaCl Atom-Thin Layer on Methylammonium Lead Iodide Perovskite: New Hints for Perovskite Solar Cells from First-Principles Calculations, *Phys. Chem. Chem. Phys.*, 2024, **26**(3), 1602–1607, DOI: **10.1039/D3CP02712K**.

12 B. Yang, J. Suo, F. Di Giacomo, S. Olthof, D. Bogachuk, Y. Kim, X. Sun, L. Wagner, F. Fu, S. M. Zakeeruddin, A. Hinsch, M. Grätzel, A. Di Carlo and A. Hagfeldt, Interfacial Passivation Engineering of Perovskite Solar Cells with Fill Factor over 82% and Outstanding Operational Stability on N–i–p Architecture, *ACS Energy Lett.*, 2021, **6**(11), 3916–3923, DOI: **10.1021/acsenergylett.1c01811**.

13 F. H. Isikgor, S. Zhumagali, L. V. T. Merino, M. De Bastiani, I. McCulloch and S. De Wolf, Molecular Engineering of Contact Interfaces for High-Performance Perovskite Solar Cells, *Nat. Rev. Mater.*, 2023, **8**(2), 89–108, DOI: **10.1038/s41578-022-00503-3**.

14 B. Dong, M. Wei, Y. Li, Y. Yang, W. Ma, Y. Zhang, Y. Ran, M. Cui, Z. Su, Q. Fan, Z. Bi, T. Edvinsson, Z. Ding, H. Ju, S. You, S. M. Zakeeruddin, X. Li, A. Hagfeldt, M. Grätzel and Y. Liu, Self-Assembled Bilayer for Perovskite Solar Cells with Improved Tolerance against Thermal Stresses, *Nat. Energy*, 2025, 1–12, DOI: **10.1038/s41560-024-01689-2**.

15 Y. Li, H. Li, C. Zhong, G. Sini and J.-L. Brédas, Characterization of Intrinsic Hole Transport in Single-Crystal Spiro-OMeTAD, *npj Flexible Electron.*, 2017, **1**(1), 1–8, DOI: **10.1038/s41528-017-0002-0**.

16 S. M. Abdalhadi, M. K. A. Mohammed, A. Y. Al-Baitai and Z. M. Yaseen, TD-DFT-Guided Development of a Robust Hole-Transporting Layer for Optimized Triple-Cation Perovskite Solar Cell Performance, *New J. Chem.*, 2024, **48**(44), 18728–18738, DOI: **10.1039/D4NJ03550J**.

17 C. Coppola, R. Infantino, A. Dessì, L. Zani, M. L. Parisi, A. Mordini, G. Reginato, R. Basosi and A. Sinicropi, DFT and TDDFT Investigation of Four Triphenylamine/Phenothiazine-Based Molecules as Potential Novel Organic Hole Transport Materials for Perovskite Solar Cells, *Mater. Chem. Phys.*, 2022, **278**, 125603, DOI: **10.1016/j.matchemphys.2021.125603**.

18 S. Jahanbani and R. Ghadari, Theoretical Study of Optoelectronic Performance of Hole-Transporting Material Quinoxaline-Based with Architecture (D-A-D) in Perovskite Solar Cells: A DFT Method, *J. Mol. Liq.*, 2024, **398**, 124296, DOI: **10.1016/j.molliq.2024.124296**.

19 R. Singh, S. Begam Elavarasi and M. Guin, Theoretical Investigation of Triphenylamine/Anthradithiophene Based Systems as Potential Organic Hole Transport Materials for Perovskite Solar Cells, *Chem. Phys. Lett.*, 2024, **836**, 141057, DOI: **10.1016/j.cplett.2023.141057**.

20 A. Pecoraro, P. Maddalena, M. Pavone and A. B. Muñoz García, First-Principles Study of Cu-Based Inorganic Hole Transport Materials for Solar Cell Applications, *Materials*, 2022, **15**(16), 5703, DOI: **10.3390/ma15165703**.

21 A. Dkhissi, D. Beljonne and R. Lazzaroni, Atomic Scale Modeling of Interfacial Structure of PEDOT/PSS, *Synth. Met.*, 2009, **159**(5), 546–549, DOI: **10.1016/j.synthmet.2008.11.022**.

22 N. Sultana, A. Al Amin, D. Z. Metin and N. Gaston, Unveiling the Structures and Electronic Properties of $CH_3NH_3PbI_3$ Interfaces with TiO_2, ZnO, and SnO_2: A First-Principles Study, *J. Mater. Sci.*, 2019, **54**(21), 13594–13608, DOI: **10.1007/s10853-019-03867-0**.

23 X.-F. Diao, Y. Tang, Q. Xie, D.-L. Chen, S. Li and G.-F. Liu, Study on the Property of Electron-Transport Layer in the Doped Formamidinium Lead Iodide Perovskite Based on DFT, *ACS Omega*, 2019, **4**(22), 20024–20035, DOI: **10.1021/acsomega.9b03015**.

24 A. Pecoraro, F. Fasulo, M. Pavone and A. B. Muñoz-García, First-Principles Study of Interfacial Features and Charge Dynamics between Spiro-MeOTAD and Photoactive Lead Halide Perovskites, *Chem. Commun.*, 2023, **59**(34), 5055–5058, DOI: **10.1039/D3CC00960B**.

25 B. Al-Anesi, G. K. Grandhi, A. Pecoraro, V. Sugathan, A. B. Muñoz-García, M. Pavone and P. Vivo, Dissecting the Role of the Hole-Transport Layer in Cu_2 $AgBiI_6$ Solar Cells: An Integrated Experimental and Theoretical Study, *J. Phys. Chem. C*, 2024, **128**(23), 9446–9453, DOI: **10.1021/acs.jpcc.4c01871**.

26 P. Han and Y. Zhang, Recent Advances in Carbazole-Based Self-Assembled Monolayer for Solution-Processed Optoelectronic Devices, *Adv. Mater.*, 2024, **36**(33), 2405630, DOI: **10.1002/adma.202405630**.

27 Z. Yi, X. Li, Y. Xiong, G. Shen, W. Zhang, Y. Huang, Q. Jiang, X. R. Ng, Y. Luo, J. Zheng, W. L. Leong, F. Fu, T. Bu and

J. Yang, Self-Assembled Monolayers (SAMs) in Inverted Perovskite Solar Cells and Their Tandem Photovoltaics Application, *Interdiscip. Mater.*, 2024, **3**(2), 203–244, DOI: 10.1002/idm2.12145.

28 M. J. Lee, J.-S. Park, T. H. Kim, M. A. Saeed, G. M. Lee and J. W. Shim, Tailoring Hole-Selective Contacts *via* Self-Assembled Monolayers for Advancing Indoor Organic Photovoltaic and Capacitor Devices, *Chem. Eng. J.*, 2024, **481**, 148481, DOI: 10.1016/j.cej.2023.148481.

29 B. Yang, J. Suo, E. Mosconi, D. Ricciarelli, W. Tress, F. De Angelis, H.-S. Kim and A. Hagfeldt, Outstanding Passivation Effect by a Mixed-Salt Interlayer with Internal Interactions in Perovskite Solar Cells, *ACS Energy Lett.*, 2020, **5**(10), 3159–3167, DOI: 10.1021/acsenergylett.0c01664.

30 I. M. Adam, K. T. Soe, W. Ruengsrisang, E. Ketsombun, T. Supasai, T. Sutthibutpong, N. Rujisamphan and N. Thongprong, SnO_2/Perovskite Interface Engineering with Mixed-Halide Potassium Salts: A Pathway to Efficient and Stable Perovskite Solar Cells through a Combined Experimental-Density Functional Theory Approach, *ACS Appl. Mater. Interfaces*, 2025, **17**(21), 31000–31012, DOI: 10.1021/acsami.5c04415.

31 D. Takhellambam, L. A. Castriotta, G. Zanotti, L. Mancini, V. Raglione, G. Mattioli, B. Paci, A. Generosi, M. Guaragno, V. Campanari, G. Ammirati, F. Martelli, E. Calabrò, A. Cricenti, M. Luce, N. Yaghoobi Nia, F. Di Giacomo and A. Di Carlo, Enhancing Hole Transfer in Perovskite Solar Cell with Self-Assembled Monolayer by Introducing [1] benzothieno [3,2-b][1]benzothiophene Interlayer, *Sol. RRL*, 2023, **7**(24), 2300658, DOI: 10.1002/solr.202300658.

32 C. Ma, M. Grätzel and N.-G. Park, Facet Engineering for Stable, Efficient Perovskite Solar Cells, *ACS Energy Lett.*, 2022, **7**(9), 3120–3128, DOI: 10.1021/acsenergylett.2c01623.

33 D. H. Cao, C. C. Stoumpos, C. D. Malliakas, M. J. Katz, O. K. Farha, J. T. Hupp and M. G. Kanatzidis, Remnant PbI_2, an Unforeseen Necessity in High-Efficiency Hybrid Perovskite-Based Solar Cells?A), *APL Mater.*, 2014, **2**(9), 091101, DOI: 10.1063/1.4895038.

34 C. Roldán-Carmona, P. Gratia, I. Zimmermann, G. Grancini, P. Gao, M. Grätzel and M. K. Nazeeruddin, High Efficiency Methylammonium Lead Triiodide Perovskite Solar Cells: The Relevance of Non-Stoichiometric Precursors, *Energy Environ. Sci.*, 2015, **8**(12), 3550–3556, DOI: 10.1039/C5EE02555A.

35 Z. Futera and J. Blumberger, Electronic Couplings for Charge Transfer across Molecule/Metal and Molecule/Semiconductor Interfaces: Performance of the Projector Operator-Based Diabatization Approach, *J. Phys. Chem. C*, 2017, **121**(36), 19677–19689, DOI: 10.1021/acs.jpcc.7b06566.

36 I. Kondov, M. Čížek, C. Benesch, H. Wang and M. Thoss, Quantum Dynamics of Photoinduced Electron-Transfer Reactions in Dye–Semiconductor Systems: First-Principles Description and Application to Coumarin 343–TiO_2, *J. Phys. Chem. C*, 2007, **111**(32), 11970–11981, DOI: 10.1021/jp072217m.

37 W. Jian, R. Jia, H.-X. Zhang and F.-Q. Bai, Arranging Strategies for A-Site Cations: Impact on the Stability and Carrier Migration of Hybrid Perovskite Materials, *Inorg. Chem. Front.*, 2020, **7**(8), 1741–1749, DOI: 10.1039/D0QI00102C.

38 K. Burke, Perspective on Density Functional Theory, *J. Chem. Phys.*, 2012, **136**(15), 150901, DOI: 10.1063/1.4704546.

39 V. Blum, R. Gehrke, F. Hanke, P. Havu, V. Havu, X. Ren, K. Reuter and M. Scheffler, Ab Initio Molecular Simulations with Numeric Atom-Centered Orbitals, *Comput. Phys. Commun.*, 2009, **180**(11), 2175–2196, DOI: 10.1016/j.cpc.2009.06.022.

40 V. Havu, V. Blum, P. Havu and M. Scheffler, Efficient O(N) Integration for All-Electron Electronic Structure Calculation Using Numeric Basis Functions, *J. Comput. Phys.*, 2009, **228**(22), 8367–8379, DOI: 10.1016/j.jcp.2009.08.008.

41 J. P. Perdew, K. Burke and M. Ernzerhof, Generalized Gradient Approximation Made Simple, *Phys. Rev. Lett.*, 1996, **77**(18), 3865–3868, DOI: 10.1103/PhysRevLett.77.3865.

42 A. Tkatchenko and M. Scheffler, Accurate Molecular Van Der Waals Interactions from Ground-State Electron Density and Free-Atom Reference Data, *Phys. Rev. Lett.*, 2009, **102**(7), 073005, DOI: 10.1103/PhysRevLett.102.073005.